Biorobotic AUV Maneuvering by Pectoral Fins: Inverse Control Design Based on CFD Parameterization

Sahjendra N. Singh, *Senior Member, IEEE*, Aditya Simha, *Student Member, IEEE*, and Rajat Mittal

***Abstract*—Biologically inspired maneuvering of autonomous undersea vehicles (AUVs) in the dive plane using pectoral-like oscillating fins is considered. Computational fluid dynamics are used to parameterize the forces generated by a mechanical flapping foil, which attempts to mimic the pectoral fin of a fish. Since the oscillating fins produce periodic force and moment of a variety of wave shapes, the essential characteristics of these signals are captured in their Fourier expansions. Maneuvering of the biorobotic AUV in the dive plane is accomplished by periodically altering the bias angle of the oscillating fin. Based on a discrete-time AUV model, an inverse control system for the dive-plane control is derived. It is shown that, in the closed-loop system, the inverse control system accomplishes accurate tracking of the prescribed time-varying depth trajectories and the segments of the intersample depth trajectory remain close to the discrete-time reference trajectory. The results show that the fins located away from the center of mass toward the nose of the vehicle provide better maneuverability.**

***Index Terms*—Biorobotic autonomous underwater vehicle (BAUV), computational fluid dynamics (CFD), inverse control, pectoral fins.**

I. Introduction

DENIZENS of the aquatic world have a splendid ability to perform swift, complex, and intricate maneuvers that employ oscillating fins [1], [2]. This has compelled researchers to design flapping foils for propulsion and control of biorobotic autonomous underwater vehicles (BAUVs) [3]–[6]. Research has been conducted on fish morphology, locomotion, and application of biologically inspired control surfaces to rigid bodies [2], [3], [6]–[8]. Extensive effort has been made to measure the forces and moments produced by oscillating fins in laboratory experiments [3], [5], [9]–[11]. Observations yield that pectoral fins undergoing a combination of lead–lag, feathering, and flapping motions also have the ability to produce large lift, side force, and thrust, which can then be used for the control and propulsion of autonomous underwater vehicles (AUVs) [8], [10], [11].

Manuscript received September 23, 2003; revised April 13, 2004. The work of S. N. Singh and A. Simha was supported by the U.S. Office of Naval Research under Grant N0014-03-1-0459. The work of R. Mittal was supported by the Office of Naval Research under Grant N00014-03-1-0458.

S. N. Singh and A. Simha are with the Department of Electrical and Computer Engineering, University of Nevada, Las Vegas, NV 89154-4026 USA (e-mail: sahaj@ee.unlv.edu).

R. Mittal is with the Department of Mechanical and Aerospace Engineering, The George Washington University, Washington DC 22052 USA (e-mail: mittal@gwu.edu).

Digital Object Identifier 10.1109/JOE.2004.833117

Computational methods have also been used in several of these studies to obtain forces and moments of flapping foils [12]–[17]. An analytical representation of the unsteady hydrodynamics of oscillating foils have been obtained using Theodorsen's theory [18]. Fuzzy controllers and neural networks have also been suggested [9]–[11]. The design of open- and closed-loop control systems of a BAUV in the dive plane using optimal control theory has been considered [19].

For time-varying trajectory control, the inversion (decoupling) control technique provides a valuable tool [20]–[22]. However, for exact output trajectory control, the system must be minimum phase. But for nonminimum phase systems, approximate trajectory control can be accomplished by constructing a modified output such that the new system is minimum phase [7], [22], [23].

Considerable research is available in the literature for the design of control systems for undersea vehicles. These conventional controllers use continuously deflecting control surfaces for maneuvering. Fish produce propulsive and maneuvering forces and moments by flapping their fins. Oscillating fins produce periodic forces. Therefore, for fish-like control of BAUVs it is of interest to develop control algorithms that are based on oscillatory (periodic) control forces.

The contribution of this paper lies in the design of an inverse control system for the time-varying depth trajectory tracking of AUVs in the dive plane using oscillating pectoral fins. It is assumed that the fins undergo a combined heaving–pitching mode of oscillation with the pitch-bias angle as the key control parameter. A Fourier series expansion of the forces and moments produced by the pectoral fins based on data obtained from computational fluid dynamics (CFD) is derived. A discrete-time model of the AUV is derived for the purpose of design. However, it turns out that the AUV model is nonminimum phase [the transfer function relating the output (depth) and input (bias angle) has unstable zeros]; therefore, one cannot design an inverse control system for exact tracking of the output trajectory. It is found that the number of unstable zeros is a function of the location of the pectoral fins on the BAUV. To overcome the obstruction created by unstable zeros, an approximate discrete-time system (that depends on the fin location) is obtained by essentially eliminating the unstable zeros from the pulse transfer function. An analytical expression of the output matrix of the approximate minimum phase system is derived. Then, an inverse control law is derived for the control of the new output variable. Interestingly, the controller designed based on the new output variable accomplishes accurate trajectory fol-

lowing of the prescribed time-varying depth trajectory. Simulation results are obtained for the tracking of sinusoidal reference depth trajectories. It is noted that the methodology developed here differs from the conventional approaches in which control surfaces are continuously deflected for control. Here, we use oscillating fins for fish-like maneuvers of BAUVs.

II. Dive-Plane Dynamics

Let the vehicle be moving in the dive plane ($X_I - Z_I$ plane) where $O_I X_I Z_I$ is an inertial coordinate system. $O_B X_B Z_B$ is a body fixed-coordinate system, X_B is in the forward direction, and Z_B points down. In the moving coordinate frame $O_B X_B Z_B$, fixed at the vehicle's geometric center, the equations of motion for neutrally buoyant vehicle are given by

$$\begin{aligned} m(\dot{w}-uq-z_G q^2-x_G\dot{q}) &= 0.5\rho l^4 z'_{\dot{q}}\dot{q}+0.5\rho l^3\left(z'_{\dot{w}}\dot{w}+z'_q qu\right) \\ &\quad +0.5\rho l^2 z'_w wu+f_{pv} \\ I_y\dot{q}+mz_G(\dot{u}+wq)-mx_G(\dot{w}-uq) &= 0.5\rho l^5 M'_{\dot{q}}\dot{q}+0.5\rho l^4\left(M'_{\dot{w}}\dot{w}+M'_q qu\right) \\ &\quad +0.5\rho l^3 M'_w wu-x_{GB}W\cos\theta \\ &\quad -z_{GB}W\sin\theta+m_{pv} \\ \dot{z} &= -u\sin\theta+w\cos\theta \end{aligned} \tag{1}$$

where θ is the pitch angle; $q = \dot{\theta}$, $x_{GB} = x_G - x_B$, $z_{GB} = z_G - z_B$, $l =$ body length, $\rho =$ density; and z is the depth. f_{pv} and m_{pv} denote the net force and moment acting on the vehicle due to the pectoral fins (see [7] and [24] for notation). The primed variables are the nondimensionalized hydrodynamic coefficients. Here, $((x_B, z_B) = 0)$ and (x_G, z_G) denote the coordinates of the center of buoyancy and center of gravity (cg), respectively. It is assumed that the forward velocity is held steady $(u = U)$ by a control mechanism. In this study, only small maneuvers of the vehicle are considered. As such linearizing the equations of motion about $w = 0, q = 0, z = 0$, and $\theta = 0$, one obtains

$$\begin{aligned} \begin{bmatrix} m-z_{\dot{w}} & -mx_G-z_{\dot{q}} & 0 \\ -mx_G-M_{\dot{w}} & I_y-M_{\dot{q}} & 0 \\ 0 & 0 & 1 \end{bmatrix}\begin{bmatrix} \dot{w} \\ \dot{q} \\ \dot{z} \end{bmatrix} &= \begin{bmatrix} z_w U & z_q+mU & 0 \\ M_w U & M_q-mx_G U & 0 \\ 1 & 0 & 0 \end{bmatrix}\begin{bmatrix} w \\ q \\ z \end{bmatrix} \\ &\quad +\begin{bmatrix} 0 \\ -z_{GB}W \\ -U \end{bmatrix}\theta+\begin{bmatrix} f_{pv} \\ m_{pv} \\ 0 \end{bmatrix} \end{aligned} \tag{2}$$

where $x_{GB} = 0$. Here, we have introduced new parameters ($z_{\dot{w}}$, $M_{\dot{q}}$, etc.), which are obtained using the nondimensionalized (primed) hydrodynamic coefficients [7], [24].

Defining the state vector $x = (w, q, z, \theta)^T \in R^4$, solving (2), one obtains a state variable representation of the form

$$\begin{aligned} \dot{x} &= Ax + B_v\begin{bmatrix} f_{pv} \\ m_{pv} \end{bmatrix} \\ y &= [0,0,1,0]x \end{aligned} \tag{3}$$

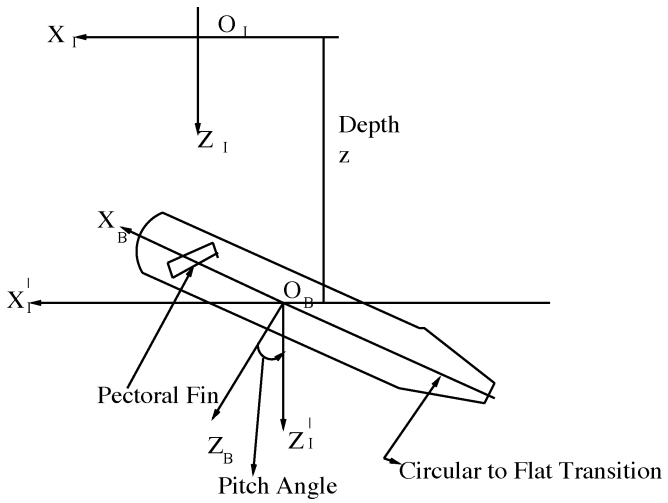

Fig. 1. Schematic of the AUV.

for appropriate matrices $A \in R^{4\times4}$ and $B_v \in R^{4\times2}$, where y (depth) is the controlled output variable.

Given a reference depth trajectory $y_r(t)$, we are interested in developing a control system so that the depth trajectory $(y(t))$ of the BAUV follows the prescribed reference trajectory $y_r(t)$.

III. Fin Force and Moment Parameterization

It is assumed that the BAUV model has one pair of pectoral fins that are arranged symmetrically around the body of the AUV. Fig. 1 shows a schematic of a typical AUV. Each fin is assumed to undergo a combined pitch-and-heave motion described as

$$h(t) = h_1\sin(\omega_f t) \tag{4}$$

$$\psi(t) = \beta_\psi + \psi_1\sin(\omega_f t+\nu_1) \tag{5}$$

where h and ψ correspond to the heave motion and pitch angle, respectively; the pitching is assumed to occur about the center-chord location. Furthermore, w_f, h_1, and ψ_1 are the frequencies and amplitudes of oscillations, β_ψ is pitch bias angle, and ν_1 is the phase difference between the pitching and heaving motions.

As a result of this flapping motion, each fin experiences a time-varying hydrodynamic force [that can be resolved into a thrust component and a lift (or pitch) component f_p] and a pitching moment m_p. The hydrodynamic forces on the pectoral fin also produce rolling and yawing moments on the BAUV, which affect its dynamics. However, since dive-plane dynamics and maneuvering is assumed to be affected by the pitching force and moment only, we limit our discussion to these components.

Since $f_p(t)$ and $m_p(t)$ are periodic functions, they can be represented by the Fourier series

$$\begin{aligned} f_p &= \sum_{n=0}^{M}\left(f_n^s\sin(nw_f t)+f_n^c\cos(nw_f t)\right) \\ m_p &= \sum_{n=0}^{M}\left(m_n^s\sin(nw_f t)+m_n^c\cos(nw_f t)\right) \end{aligned} \tag{6}$$

where it is assumed that the fins produce dominant M harmonically related components and the harmonics of higher frequencies are negligible. The Fourier coefficients f_n^a and m_n^a, $a \in \{s, c\}$, capture the characteristics of the time-varying signals $f_p(t)$ and $m_p(t)$. Parameterization of these coefficients is, therefore, needed in order to complete the equations that govern the motion of the BAUV in the dive plane.

The following are the key nondimensional parameters that govern the performance of a rigid, rectangular, flapping foil: Re, St, β_ψ, ψ_1, ν_1, h_1/c, and s/c where $Re = cU_\infty/\nu$, $St = z_1\omega/\pi U_\infty$, c is the foil chord and s is the foil span. For simplicity, a quasi-steady assumption has often been employed in order to relate the hydrodynamic and aerodynamic forces to the foil parameters [18], [25]. For instance, the lift on a pitching-heaving foils has been estimated as [25]

$$f_p(t) = \rho U_\infty^2 c_{l_\alpha} \left[\alpha + \frac{\dot{h}}{U_\infty} + K\left(\frac{\dot{\alpha}}{U_\infty}\right)\right] \tag{7}$$

where α denotes the instantaneous angle of attack, c_{l_α} is the lift coefficient per unit angle of attack, and K is a known constant. The above parameterization assumes that the instantaneous lift force generated by a flapping foil is equal to that produced by a static foil at an equivalent angle of attack. This is a reasonable approximation for low amplitude wing flutter, where such approximations have been employed in the past. However, it is well known [26], [27] that unsteady mechanisms dominate the flow over flapping foils undergoing large amplitude motions and that quasi-steady estimates can be significantly erroneous. In the current effort, we therefore conduct a first-of-its-kind study where CFD is used to parameterize the performance of these flapping foils.

In order to understand the scope of this problem, consider that the force coefficients f_n^s, f_n^c, m_n^s, and m_n^c are function of all the major nondimensional parameters; that is, for some function $\gamma_{nga}(n = 0, \ldots, M)$

$$g_n^a = \gamma_{nga}\left(\beta_\psi, \psi_1, \nu_1, St, \frac{h_1}{c}, \mathrm{Re}, \frac{s}{c}\right) \tag{8}$$

where $g \in \{f, m\}$ and $a \in \{s, c\}$. It should be noted that the first five parameters in (8) (β_ψ, ψ_1, ν_1, St, and h_1/c) could be employed to control the trajectory and motion of the BAUV. The Reynolds number parameter, on the other hand, depends on the velocity of the BAUV relative to the surrounding fluid and is controlled primarily by the main propulsor. Finally, the last parameter s/c is a design parameter and is assumed to be fixed for a given pectoral fin. Thus, a complete parameterization of the performance of the flapping foil for the BAUV conceptual model requires that the CFD simulations extract the dependence of the force coefficients on the first four parameters as well as the Reynolds number.

Clearly, these five parameters represent a large parameter space, which pose a significant challenge to any CFD based parameterization effort. However, our focus on the dive-plane maneuvering and dynamics allows us to narrow the scope of the problem. Maneuvering in the dive plane requires manipulation of only the pitching force and moment; it is plausible to accomplish this through the variation of only one control input. Indeed, the recent experimental study of [28] indicates that the pitch-bias angle β_ψ would be an appropriate parameter for affecting such maneuvers. Motivated by this, we have chosen β_ψ as the primary control variable and have proceeded to extract the dependence of foil performance on this parameter through CFD.

A Cartesian grid method [13]–[15] is employed for the current simulations. The distinguishing feature of this method is that the governing equations are discretized on a Cartesian grid, which does not conform to the immersed boundary. This greatly simplifies grid generation and also retains the relative simplicity of the governing equations in Cartesian coordinates. Therefore, this method has distinct advantages over the conventional body-fitted approach in simulating flows with moving boundaries and/or complicated shapes [29]. The framework of this method can be considered to be Eulerian–Lagrangian, wherein the immersed boundaries are explicitly tracked as surfaces in a Lagrangian fashion, while the flow computations are performed on a fixed Eulerian mesh. The method employs a second-order central difference scheme in space and a second-order accurate fractional-step method for time advancement.

IV. Discrete-Time Representation

In this section, the design of a dive-plane feedback control law is considered. We assume that bias angle (control input) $\beta = \beta_\psi$ is varied periodically and that the remaining oscillation parameters are constant. It has been experimentally shown that the mean values of the normal force and the pitching moment vary almost linearly with β and that the amplitudes of the fin force and moment are functions of β [5], [28].

Expanding the fin force and moment of each fin in a Taylor series about $\beta = 0$ gives

$$\begin{aligned} f_p(t,\beta) &= f_p(t,0) + \frac{\partial f_p}{\partial \beta}(t,0)\beta + O(\beta^2) \\ m_p(t,\beta) &= m_p(t,0) + \frac{\partial m_p}{\partial \beta}(t,0)\beta + O(\beta^2) \end{aligned} \tag{9}$$

where $O(\beta^2)$ denotes higher order terms. We assume here that for a fixed $\beta \in R$, $f_p(t+T_0, \beta) = f_p(t, \beta)$, and $m_p(t+T_0, \beta) = m_p(t, \beta)$, $t > 0$ (T_0 denotes the fundamental period). Then, the partial derivatives of f_p and m_p with respect to β are also periodic functions of time. Using (6), one can approximately express f_p and m_p as

$$\begin{aligned} f_p &= \sum_{n=0}^{M} f_n^s(0)\sin nw_f t + f_n^c(0)\cos nw_f t \\ &\quad + \sum_{n=0}^{M}\left(\frac{\partial f_n^s}{\partial \beta}(0)\sin nw_f t + \frac{\partial f_n^c}{\partial \beta}(0)\cos nw_f t\right)\beta \\ m_p &= \sum_{n=0}^{M} m_n^s(0)\sin nw_f t + m_n^c(0)\cos nw_f t \\ &\quad + \sum_{n=0}^{M}\left(\frac{\partial m_n^s}{\partial \beta}(0)\sin nw_f t + \frac{\partial m_n^c}{\partial \beta}(0)\cos nw_f t\right)\beta \end{aligned} \tag{10}$$

where $O(\beta^2)$ terms are ignored in the series expansion. We define

$$\begin{aligned} f_a &= \left(f_0^c(0), f_1^s(0), f_1^c(0), \ldots, f_M^s(0), f_M^c(0)\right)^T \\ f_b &= \left(\frac{\partial f_0^c}{\partial \beta}(0), \frac{\partial f_1^s}{\partial \beta}(0), \frac{\partial f_1^c}{\partial \beta}(0), \ldots, \frac{\partial f_M^s}{\partial \beta}(0), \frac{\partial f_M^c}{\partial \beta}(0)\right)^T \\ m_a &= \left(m_0^c(0), m_1^s(0), m_1^c(0), \ldots, m_M^s(0), m_M^c(0)\right)^T \\ m_b &= \left(\frac{\partial m_0^c}{\partial \beta}(0), \frac{\partial m_1^s}{\partial \beta}(0), \ldots, \frac{\partial m_M^s}{\partial \beta}(0), \frac{\partial m_M^c}{\partial \beta}(0)\right)^T \end{aligned} \quad (11)$$

where $f_a, f_b, m_a, m_b \in R^{2M+1}$. Using (10) and (11), we get

$$\begin{aligned} f_p(t) &= \phi^T(f_a + \beta f_b) \\ m_p(t) &= \phi^T(m_a + \beta m_b) \\ \phi &= [1 \ \sin w_f t \ \ldots \sin M w_f t \ \cos M w_f t]^T. \end{aligned} \quad (12)$$

The vehicle has two attached fins; therefore, the net force and moment are $f_{pv} = -2f_p$ and $m_{pv} = 2(d_{cgf} f_p + m_p)$, where d_{cgf} is the moment arm due to the fin location (positive forward). The dive-plane dynamics (3) can be written as

$$\dot{x} = Ax + B\Phi(t) f_c + B\Phi(t) f_v \beta \quad (13)$$

where $B[f_p, m_p]^T = B_v[f_{pv}, m_{pv}]^T$, $f_c = (f_a^T, m_a^T)^T \in R^{4M+2}$, and $f_v = (f_b^T, m_b^T)^T \in R^{4M+2}$, where

$$\Phi(t) = \begin{bmatrix} \phi^T(t) & 0 \\ 0 & \phi^T(t) \end{bmatrix}. \quad (14)$$

For the purpose of control, the bias angle is periodically changed at a sampling interval of T^*, where T^* is an integer multiple of the period T_0, i.e., $T^* = n_0 T_0$, where n_0 is a positive integer. In this way, one switches the bias angle at an uniform rate of T^* seconds at the end of n_0 cycles.

For the derivation of the control law, the transients introduced due to switching are ignored in this study. Since the bias is changed periodically, it will be convenient to express the continuous-time system (13) as a discrete-time system. The function $\beta(t)$ now has piecewise constant values β_k for $t \in [kT^*, (k+1)T^*)$, $k = 0, 1, 2 \ldots$. The solution of (13) is given by

$$x(t) = e^{A(t-t_0)} x(t_0) + \int_{t_0}^{t} e^{A(t-\tau)} B\Phi(\tau) \left[f_c + f_v \beta(\tau)\right] d\tau. \quad (15)$$

Taking $t_0 = kT^*$ and $t = (k+1)T^*$, one has

$$\begin{aligned} x\left[(k+1)T^*\right] &= e^{AT^*} x(kT^*) \\ &\quad + \int_{kT^*}^{(k+1)T^*} e^{A[(k+1)T^* - \tau]} B\Phi(\tau)[f_c + f_v \beta_k] d\tau. \end{aligned} \quad (16)$$

Let $(k+1)T^* - \tau = s$. Then, noting that

$$\Phi\big((k+1)T^* - s\big) = \Phi(-s) \quad (17)$$

(15) gives

$$\begin{aligned} x\left[(k+1)T^*\right] &= e^{AT^*} x(kT^*) + \int_0^{T^*} e^{As} B\Phi(-s)[f_c + f_v \beta_k] ds \\ &\doteq A_d x(kT^*) + B_d \beta_k + d \end{aligned} \quad (18)$$

where $A_d = e^{AT^*}$ and $B_0 = \int_0^{T^*} e^{As} B\Phi(-s) ds$, $B_d = B_0 f_v \in R^4$, and $d = B_0 f_c \in R^4$.

The output variable (z) is

$$y(kT^*) = [0 \quad 0 \quad 1 \quad 0] x(kT^*) \doteq C_d x(kT^*). \quad (19)$$

The transfer function relating the output $y(kT^*)$ and the input β_k (assuming that $d = 0$) is given by

$$\begin{aligned} \frac{\hat{y}(z)}{\hat{\beta}(z)} &= G(z) \\ &= C_d (zI - A_d)^{-1} B_d \\ &= k_p \frac{(z+\mu_1)(z+\mu_2)(z+\mu_3)}{z^4 + a_3 z^3 + a_2 z^2 + a_1 z + a_0} \end{aligned} \quad (20)$$

where z denotes the Z-transform variable, $\mu_i (i = 1, 2, 3)$ are real or complex numbers, and k_p and $a_i (i = 0, 1, 2, 3)$ are real numbers.

It is assumed that the pectoral fins are attached between the cg and the nose of the vehicle. For the AUV model under consideration, the number of unstable zeros (i.e., the zeros outside the unit disk in the complex plane) depends on the distance (d_{cgf}) of the pectoral fins from the cg. It has been found that there exists a single unstable zero if the fins are attached closer to the cg, but two unstable zeros appear if the attachment distance d_{cgf} exceeds a critical value. Thus, the transfer function $G(z)$ has at least one unstable zero and is nonminimum phase. Of course, the continuous-time AUV model has only two zeros, but the pulse transfer function $G(z)$ has three zeros. For this nonminimum phase AUV model, it is not possible to synthesize an inverse controller. Here, we modify the controlled output variable so that the new transfer function is minimum phase and then derive the inverse control law for approximate depth trajectory control.

V. Minimum Phase System

In this section, the derivation of a minimum phase approximate model for an nth-order single-input–single-output (SISO) nonminimum phase system is considered. For this purpose, the original transfer function is simplified by ignoring its unstable zeros. We consider a SISO of the form (18) and (19) with $d = 0$ (denoted as (A_d, B_d, C_d)), where $x \in R^n$, $A_d \in R^{n \times n}$, and suppose that the system has q_s stable and q_u unstable zeros. The transfer function relating the output $y(kT^*)$ and the input β_k of the system (A_d, B_d, C_d) (assuming that $d = 0$) is

$$\frac{\hat{y}(z)}{\hat{\beta}(z)} = G(z) = C_d (zI - A_d)^{-1} B_d = \frac{n_d(z)}{\Delta(z)} \quad (21)$$

where the nth-order characteristic polynomial $\Delta(z)$ is

$$\Delta(z) = \det[zI - A_d] = z^n + a_{n-1} z^{n-1} + \ldots + a_1 z + a_0 \quad (22)$$

and the numerator polynomial is

$$n_d(z) = k_p \prod_{j=1}^{q_u}(z+\mu_{uj}) \prod_{j=1}^{q_s}(z+\mu_{sj}) \tag{23}$$

where a_i $(i = 0, 1, \ldots, n-1)$ and k_p are constants and $-\mu_{uj}(j = 1, \ldots, q_u)$ and $-\mu_{sj}(j = 1, \ldots, q_s)$ are unstable and stable zeros of the transfer function; that is, $|\mu_{uj}| > 1$ and $|\mu_{sj}| < 1$.

For obtaining a minimum phase-approximate system, one removes the unstable zeros of $G(z)$ but retains the zero-frequency [direct current (dc)] gain. Thus, the approximate transfer function $G_a(z)$ takes the form

$$\begin{aligned} G_a(z) &= k_p \Delta^{-1}(z) \prod_{j=1}^{q_u}(1+\mu_{uj}) \prod_{j=1}^{q_s}(z+\mu_{sj}) \\ &= (h_{qs} z^{q_s} + \ldots + h_1 z + h_0)\Delta^{-1}(z). \end{aligned} \tag{24}$$

The approximate transfer function $G_a(z)$ now has q_s stable zeroes, but the poles of $G_a(z)$ and $G(z)$ coincide.

We are interested in deriving a new controlled output variable y_a such that

$$y_a(kT^*) = C_a x(kT^*) \tag{25}$$

and

$$\frac{\hat{y}_a(z)}{\hat{\beta}(z)} = G_a(z) = C_a(zI_n - A_d)^{-1}B_d \tag{26}$$

where C_a is a new output matrix that is yet to be determined. Using the expression of the resolvent matrix [inverse of $(zI_n - A_d)$], one can write $G_a(z)$ as [30]

$$\begin{aligned} G_a(z) = \Delta^{-1}(z) \big[&(z^{n-1} + a_{n-1}z^{n-2} + \ldots + a_1)C_aB_d \\ &+ (z^{n-2} + a_{n-1}z^{n-3} + \ldots a_2)C_aA_dB_d \\ &+ \ldots + (z + a_{n-1})C_aA_d^{n-2}B_d \\ &+ C_aA_d^{n-1}B_d \big]. \end{aligned} \tag{27}$$

The relative degree r of $G_a(z)$ is $r = n - q_s$ and, therefore, one must have

$$\begin{aligned} C_aA_d^jB_d &= 0, \qquad j = 0, 1, \ldots, r-2 \\ C_aA_d^{r-1}B_d &\neq 0. \end{aligned} \tag{28}$$

Using (28) in (27) gives

$$\begin{aligned} G_a(z) = \Delta^{-1}(z) &\\ \times \big[&(z^{n-r} + a_{n-1}z^{n-r-1} + \ldots + a_r)C_aA_d^{r-1}B_d \\ &+ \ldots + (z + a_{n-1})C_aA_d^{n-2}B_d \\ &+ C_aA_d^{n-1}B_d \big]. \end{aligned} \tag{29}$$

Noting that $q_s = n - r$, using (28) and equating the numerator polynomials of (24) and (29) gives

$$\begin{aligned} C_aA_d^{r-1}B_d &= h_{q_s} \\ C_aA_d^rB_d + a_{n-1}C_aA_d^{r-1}B_d &= h_{q_s-1} \\ &\vdots \\ C_aA_d^{n-2}B_d + a_{n-1}C_aA_d^{n-3}B_d & \\ + \ldots + a_{r+1}C_aA_d^{r-1}B_d &= h_1 \\ C_aA_d^{n-1}B_d + a_{n-1}C_aA_d^{n-2}B_d & \\ + \ldots + a_rC_aA_d^{r-1}B_d &= h_0. \end{aligned} \tag{30}$$

Collecting (28) and (30), one obtains the matrix equation

$$C_aL = h_f \tag{31}$$

where $h_f = [0, 0, \ldots, 0, h_{qs}, h_{q_s-1}, ., h_1, h_0]$ and the $n \times n$ matrix L is obtained by comparing matrix equation (31) with (30). Assuming that the system (18) is controllable, one has that rank $[B_d, A_dB_d, \ldots, A_d^{n-1}B_d] = n$ [31]. In view of (31), it follows that the columns of L are independent. Then, solving (31) gives

$$C_a = h_fL^{-1}. \tag{32}$$

To this end, a question arises: How close is the new output $y_a(kT^*)$ to $y(kT^*)$? In view of (21) and (24), it is seen that the modified output $y_a(kT^*)$ and the actual depth $y(kT^*)$ are related as

$$\hat{y}(z) = \prod_{j=1}^{q_u}(z+\mu_{uj})(1+\mu_{uj})^{-1}\hat{y}_a(z) \doteq G_f(z)\hat{y}_a(z). \tag{33}$$

According to (33), the actual output is obtained by passing $\hat{y}_a(z)$ through a filter that has the frequency response (amplitude and phase response) given by

$$G_f\left(e^{j\omega T^*}\right) = \prod_{j=1}^{q_u}\left(e^{j\omega T^*} + \mu_{uj}\right)(1+\mu_{uj})^{-1}. \tag{34}$$

Apparently, if the zero locations μ_{uj} and the frequency ωT^* are such that

$$\left(e^{j\omega T^*} + \mu_{uj}\right) \approx 1 + \mu_{uj}, \qquad j = 1, \ldots, q_u \tag{35}$$

then it follows that

$$G_f\left(e^{j\omega T^*}\right) \approx 1. \tag{36}$$

That is, the gain of $G_f(z)$ is 1 and

$$y(kT^*) \approx y_a(kT^*). \tag{37}$$

When $y_a(kT^*)$ asymptotically converges to a constant value y_r^*, one can take $\omega = 0$ and, in this case, the actual output y converges to y_r^*. Thus, it follows that if (36) is valid, then the synthesis of the inverse controller designed for the trajectory control of the modified output y_a accomplishes accurate control of the depth trajectory. In the next section, an inverse control law is designed for the tracking control of the modified output y_a.

VI. Inverse Control Law

Now consider a new system

$$\begin{aligned} x\left[(k+1)T^*\right] &= A_d x(kT^*) + B_d\beta_k + d \\ y_a(kT^*) &= C_a x(kT^*) \end{aligned} \tag{38}$$

where $x \in R^n$, $y_a(kT^*)$, and β_k are scalars and the output $y_a(kT^*)$ is the modified value of $y(kT^*)$. Suppose that a reference trajectory $y_r(kT^*)$ is given, which is to be tracked by $y_a(kT^*)$. In view of (38), using it recursively one has that

$$y_a\left[(k+1)T^*\right] = C_a A_d x(kT^*) + C_a d \tag{39}$$

$$\vdots$$

$$y_a\left[(k+r-1)T^*\right] = C_a A_d^{r-1} x(kT^*) + \sum_{i=0}^{r-2} C_a A_d^i d$$

$$\begin{aligned} y_a\left[(k+r)T^*\right] &= C_a A_d^r x(kT^*) + \sum_{i=0}^{r-1} C_a A_d^i d \\ &\quad + C_a A_d^{r-1} B_d \beta_k. \end{aligned} \tag{40}$$

The system has relative degree r. Therefore, the input β_k appears for the first time in $y_a[(k+i)T^*]$ for $i = r$.

We are interested in tracking the reference trajectory $y_r(kT^*)$. For this purpose, we choose the control input β_k as

$$\beta_k = \left(C_a A_d^{r-1} B_d\right)^{-1} \left[-C_a A_d^r x(kT^*) - \sum_{i=0}^{r-1} C_a A_d^i d + v_k\right] \tag{41}$$

where the signal v_k is selected as

$$\begin{aligned} v_k = y_r\left[(k+r)T^*\right] - \sum_{i=0}^{r-1} p_i \Bigg(& C_a A_d^i x(kT^*) \\ & + \sum_{j=0}^{i-1} C_a A_d^i d - y_r\left[(k+i)T^*\right] \Bigg) \end{aligned} \tag{42}$$

where p_i $(i = 0, 1, \ldots r-1)$ are real numbers. Defining the tracking error $e(kT^*) = y_a(kT^*) - y_r(kT^*)$ and using the control law (41) and (42) in (40) gives

$$\begin{aligned} e\left[(k+r)T^*\right] + p_{r-1} e\left[(k+r-1)T^*\right] + \ldots \\ + p_1 e\left[(k+1)T^*\right] + p_0 e(kT^*) = 0. \end{aligned} \tag{43}$$

The tracking error satisfies an rth-order difference equation. The characteristic polynomial associated with (43) is

$$(z^r + p_{r-1} z^{r-1} + \ldots + p_0) = 0. \tag{44}$$

The parameters p_i are chosen such that the roots of (44) are strictly within the unit disk. Then, it follows that for any initial condition $x(0)$, $e(kT^*) \to 0$ as $k \to \infty$ and the controlled output $y_a(kT^*)$ asymptotically converges to the reference sequence $y_r(kT^*)$. Furthermore, as described in the previous section, according to (36) for slowly varying $y_r(kT^*)$, $y(kT^*)$ follows $y_r(kT^*)$ accurately.

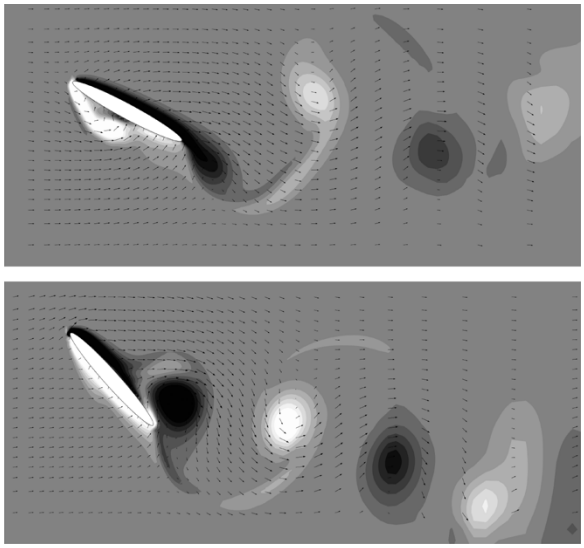

Fig. 2. Spanwise vorticity contours and velocity vectors for flow past the flapping foil for two different bias angles of 0° and 20°. Note that velocity vectors are shown on every fourth grid point in either direction.

VII. Simulation Results

A. CFD Parameterization

In the current simulations we employ a two-dimensional (2-D) $(s/c = \infty)$ 12% thick foil with an elliptic cross section. The Reynolds number is fixed at a relatively low value of 300, which alleviated the grid requirements for the simulation. In addition, h_1/c, ψ_1, ν_1, and St are fixed at value equal to 0.35, 30°, 90°, and 0.4, respectively. A nonuniform 161×111 Cartesian mesh is employed in the simulations where the grid is clustered in the region around the flapping foil and in the foil wake.

Fig. 2 shows the computed flow for the $\beta_\psi = 0°$ and 20° cases at the time instant when the foil is at the center of its heave motion. The plots show contours of spanwise vorticity (which is the curl of the velocity field) as well as the velocity vectors. For $\beta_\psi = 0°$, it is observed that the flapping foil produces a vortex street in the wake, which is comprised of counter-rotating vortices. The occurrence of such vortex streets is quite well known [32] for these flows. The vortex street is along the direction of the flow and produces a jet-like flow in the streamwise direction. For the $\beta_\psi = 20°$ flow, the vortex street it oriented at an angle to the freestream and results in a vectored jet.

Fig. 3 shows the time variation of the resultant pitching force (f_p) and moment (m_p) on the foils for these two cases. These quantities are presented as nondimensional coefficients wherein the force and moment are nondimensionalized by $q_\infty c$ and $q_\infty c^2$ with $q_\infty = (1/2)\rho U_\infty^2$. The plots clearly show that both the force and moment are periodic in time with the magnitude of variation in the pitching force being much larger than that of the moment. These force and moment coefficients can then be decomposed into their Fourier decomposition. Tables I and II

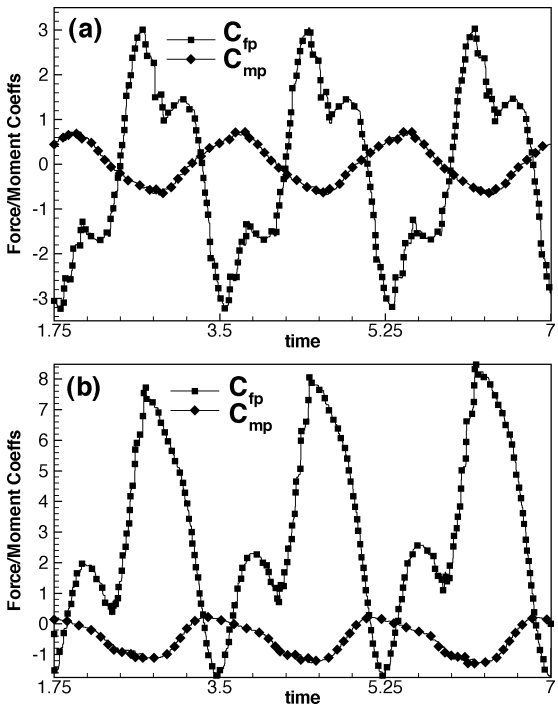

Fig. 3. Fin force and moment for (a) $\beta_\psi = 0$ and (b) $\beta_\psi = 20$ (deg).

show the nondimensionalized force and moment coefficients for the bias of zero and 20°, respectively.

In addition to these two cases, two other cases with $\beta_\psi = 10°$ and 30° have been simulated (data not shown here) and these data are used in the simulation of the BAUV dynamics, as described in the subsequent section.

B. Dive-Plane Trajectory Control

In this section, simulation results using MATLAB and SIMULINK are presented. The parameters of the model are taken from [7]. The key vehicle parameters are $l = 1.282$ m, mass $= 4.1548$ kg, $I_y = 0.5732$ kg $\cdot$ m^2, $x_G = 0$, and $z_G = 0.578\,802e-8$; the hydrodynamic parameters are taken as $z'_{\dot q} = -0.825e-5$, $z'_{\dot w} = -0.825e-5$, $z'_q = -0.238e-2$, $z'_w = -0.738e-2$, $M'_{\dot q} = -0.16e-3$, $M'_{\dot w} = -0.825e-5$, $M'_q = -0.117e-2$, and $M'_w = 0.314e-2$. The uniform forward velocity of the vehicle is 0.7 m/s. Two cases [(S1) and (S2)] of pectoral fin attachments are considered. In (S1), fins are attached at a distance of $d_{cgf} = 0.15$ m ahead of the cg. In (S2), $d_{cgf} = 0$. The fins are assumed to undergo heaving and pitching motion and the frequency of oscillation is taken to be 4 Hz [$\omega_f = 25.1327$ rad/s]. Thus, the period of oscillation is $T_0 = 0.25$ s, but the sampling period is taken as $T^* = 0.5$ s (twice the period of oscillation). The initial condition chosen is $x(0) = 0$.

Smooth reference trajectories are generated by command generators for cases (S1) and (S2), which are

$$(E^4 + p_{c3}E^3 + p_{c2}E^2 + p_{c1}E + p_{c0})y_r(kT^*) = (1 + p_{c0} + p_{c1} + p_{c2} + p_{c3})Y^*(kT^*)$$

and

$$(E^3 + p_{c2}E^2 + p_{c1}E + p_{c0})y_r(kT^*) = (1 + p_{c0} + p_{c1} + p_{c2})Y^*(kT^*)$$

TABLE I
VARIOUS COMPONENTS OF FORCE AND MOMENT COEFFICIENT FOR THE $\beta_\psi = 0°$ CASE

n	f_n^c	f_n^s	m_n^c	m_n^s
0	0.00	0.00	0.00	0.00
1	-1.89	-1.56	0.52	0.35
2	0.03	-0.04	0.00	0.01
3	-0.93	-0.08	-0.06	0.00
4	0.00	0.00	0.00	0.01

TABLE II
VARIOUS COMPONENTS OF FORCE AND MOMENT COEFFICIENT FOR THE $\beta_\psi = 20°$ CASE

n	f_n^c	f_n^s	m_n^c	m_n^s
0	2.97	0.0	-0.47	0.0
1	-2.93	-2.00	0.69	0.07
2	-0.81	1.58	-0.02	-0.13
3	-0.84	-0.21	-0.07	-0.04
4	0.09	0.22	0.02	0.02

where E denotes the advance operator ($Ey_r(kT^*) = y_r[(k+1)T^*]$) and the parameters p_{ci} are chosen to be zero so that the poles of the command generator are at $z = 0$. These two reference trajectory generators are simulated using their state variable forms with states $x_r = (x_{r1}, x_{r2}, x_{r3}, x_{r4})^T$ and $x_r = (x_{r1}, x_{r2}, x_{r3})^T$, respectively. For generating sinusoidal reference trajectories, the command input chosen is $Y^*(kT^*) = d^* \sin(\omega_r kT^*)$, where $\omega_r = 0.2$ rad/s and $d^* = 1$ m is the amplitude of the sinusoidal depth trajectory. The initial condition of the command generator is $x_r(0) = 0$. The Fourier series representations of the fin force and moment obtained using CFD have four dominant harmonics; therefore, one has $\phi(t) = [1, \sin(w_f t), \cos(w_f t), \ldots, \sin(4w_f t), \cos(4w_f t)^T$. Of course, the design approach does not limit the number of harmonics for control law derivation. The Fourier coefficients in (10) and (11) that are derived using CFD are used for simulation.

The zeros of the pulse transfer function depend on the fin attachment distance $d_{cgf} \in [0, 0.2]$ m. The transfer function $G(z)$ for case (S1) has the zeros at -1.0206, 0.2343, and 1.2731, but for (S2), the zeros are 0.8695, 1.5464, and 0.3299.

The new output y_a in (25) is computed using the solution of (32). For the AUV model, the relative degree r of the modified output for (S1) is three, but for (S2) is two; therefore, the control law (41) depends on the fin location and they are not identical for cases (S1) and (S2). For case (S1), the tracking error equation takes the form

$$(E^3 + p_2E^2 + p_1E + p_0)e(kT^*) = 0$$

but for case (S2) one has second-order error dynamics

$$(E^2 + p_1E + p_0)e(kT^*) = 0$$

where for simulation it is assumed that for (S1) $p_0 = 0.001$, $p_1 = 0.03$, and $p_1 = 0.3$. For (S2), $p_0 = 0.01$ and $p_1 = 0.2$. This gives the poles of the error dynamics at $z = -0.1$ for each case, which are well within the unit disk in the complex plane.

C. Sinusoidal Trajectory Control (S1) and (S2)

The sinusoidal reference trajectory is generated by setting $Y^*(kT^*) = d^* \sin(0.2kT^*)$ as the depth command input with $d^* = 1$ m. For case (S1), the fin oscillation period, sampling

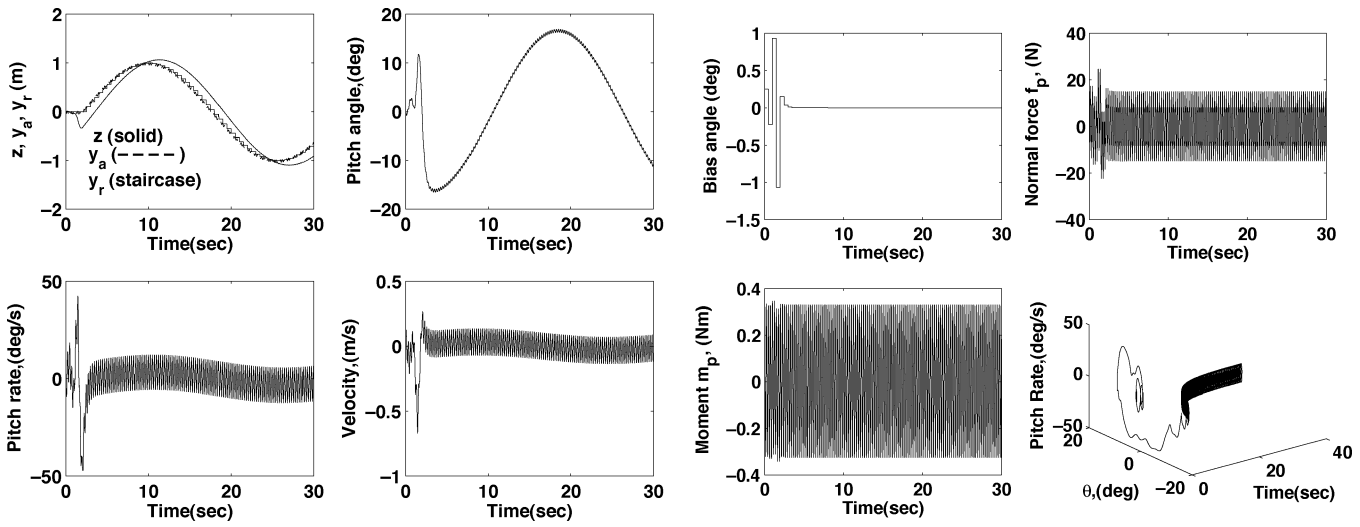

Fig. 4. Sinusoidal trajectory control case (S1).

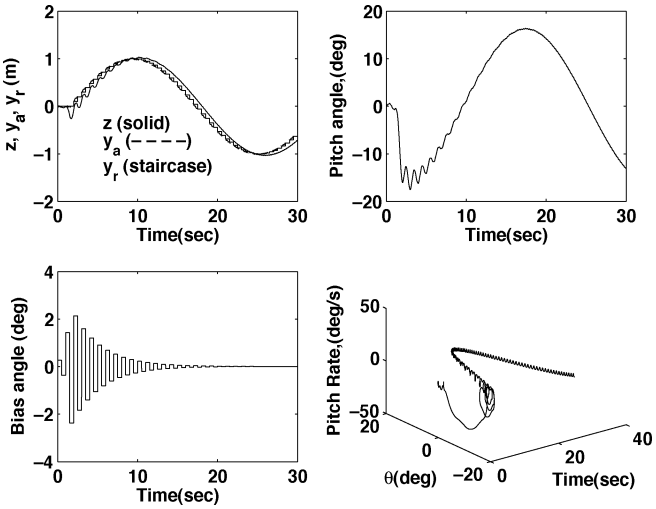

Fig. 5. Sinusoidal trajectory control case (S2).

period, and d_{cgf} are taken as 0.25 s, 0.5 s, and 0.15 m. The responses are shown in Fig. 4. We observe that the response of the modified output $\left(y_a(kT^*)\right)$ converges quickly to the command trajectory $y_r(kT^*)$. The actual depth, modified depth, and reference trajectories remain very close. The depth response in the intersample period has oscillations of minor amplitudes, but it tracks the command trajectory. The maximum pitch angle and pitch rate are less than 20° and 50°/s, respectively, and the maximum value of w does not exceed 0.75 m/s. The maximum bias angle is about 1.2°. The control force is about 30 N and the control moment is less that 0.4 Nm.

Simulation is performed using a different value of $d_{cgf} = 0$ for case (S2). Fig. 5 shows the selected responses. We observe that the controller accomplishes accurate trajectory control. The depth response is smoother, but the bias angle is larger. Furthermore, the bias angle undergoes more switchings.

VIII. Conclusion

In this paper, biologically inspired maneuvering of a biorobotic AUV using pectoral-like fins was considered. The pitch bias was updated at regular intervals (multiple of the fundamental period). CFD and Fourier series expansion were used to parameterize the effect of this control input on the hydrodynamical force and moment produced by the flapping foil. For the purpose of design, a discrete-time model was obtained and a nonminimum phase representation was derived for controller design. Then, an inverse control law for the trajectory control of the modified output was derived. In the closed-loop system, the modified output and the actual depth trajectory are sufficiently close to the desirable depth commands. Numerical results for the sinusoidal reference trajectory tracking were obtained. From these results, one concludes that accurate depth control along time-varying paths with desirable pitch angle response can be accomplished using oscillating fins. Interestingly, the control system gave better performance when the fins were attached away from the cg toward the nose.

Acknowledgment

The authors would like to sincerely thank Dr. P. R. Bandyopadhyay for providing many useful suggestions for this research.

References

[1] A. Azuma, *The Bio-Kinetics of Flying and Swimming*. New York: Springer-Verlag, 1992.

[2] M. Sfakiotakis, D. M. Lane, and J. B. C. Davies, "Review of fish swimming modes for aquatic locomotion," *IEEE J. Oceanic Eng.*, vol. 24, pp. 237–253, Apr. 1999.

[3] P. R. Bandyopadhyay, J. M. Castano, J. Q. Rice, R. B. Philips, W. H. Nedderman, and W. K. Macy, "Low-speed maneuvering hydrodynamics of fish and small underwater vehicles," *ASME J. Fluids Eng.*, vol. 119, pp. 136–144, 1997.

[4] G. S. Triantafyllou and M. S. Triantafyllou, "An efficient swimming machine," *Sci. Amer.*, vol. 272, pp. 64–70, 1995.

[5] C. B. Martin, F. S. Hover, and M. S. Triantafyllou, "Maneuvering performance of a rolling and pitching wing untethered submersible technology," presented at the 12th Int. Symp. UAVs, Durham, NH, 2001.

[6] P. R. Bandyopadhyay, J. M. Castano, and J. Dick, "Biologically-inspired bodies under surface waves—Part 1: Load measurement," *ASME J. Fluids Eng.*, vol. 121, pp. 469–478, 1999.

[7] P. R. Bandyopadhyay, S. N. Singh, and F. Chockalingam, "Biologically-inspired bodies under surface waves—Part 2: Theoretical control of maneuvering," *ASME J. Fluids Eng.*, vol. 121, pp. 479–487, 1999.

[8] P. R. Bandyopadhyay, "Manuevering hydrodynamics of fish and small underwater vehicles," *Integr. Comp. Biol.*, vol. 42, pp. 102–117, 2002.
[9] I. Yamamoto, Y. Terada, T. Nagamatu, and Y. Imaizumi, "Propulsion system with flexible/rigid oscillating fin," *IEEE J. Oceanic Eng.*, vol. 20, pp. 23–30, Apr. 1995.
[10] N. Kato, "Pectoral fin controllers," in *Neurotechnology for Biometric Robots*. Cambridge, MA: MIT Press, 2002, pp. 325–350.
[11] ——, "Perfomance in the horizontal plane of a fish robot with mechanical pectoral fins," *IEEE J. Oceanic Eng.*, vol. 25, pp. 121–129, Jan. 2000.
[12] R. Mittal, Y. Utturkar, and H. S. Udaykumar, "Computational modeling and analysis of biometric flight mechanisms," in *Proc. AIAA 40th Aerospace Sciences Meeting and Exhibit*, Reno, NV, Jan. 2002, AIAA 2002-0865.
[13] H. S. Udaykumar, R. Mittal, P. Rampunggoon, and A. Khanna, "A sharp interface Cartesian grid method for simulating flows with complex moving boundaries," *J. Comput. Phys.*, vol. 174, pp. 345–380, 2001.
[14] T. Ye, R. Mittal, H. S. Udaykumar, and W. Shyy, "An accurate cartesian grid method for simulation of viscous incompressible flows with complex immersed boundaries," *J. Comput. Phys.*, vol. 156, pp. 209–240, 1999.
[15] F. M. Najjar, R. Mittal, P. Rampunggoon, and A. Khanna, "Simulations of complex flows and fluid-structure interaction problems on fixed Cartesian grids," in *Proc. ASME–JSME Joint Fluids Engineering Conf.*, Honolulu, HI, July 2003, FEDSM2003-45 577.
[16] R. Ramamurti, R. Lohner, and W. Sandberg, "Computation of the unsteady-flow past a tuna with caudal fin oscillation," *Adv. Fluid Mech. Ser.*, vol. 9, pp. 169–178, 1996.
[17] J.-S. Lee, C. Kim, and O.-H. Rho, "The modification of airfoil shape for optimal aerodynamic performance on flapping-airfoil in low Reynolds number flow," in *AIAA 41st Aerospace Sciences Meeting and Exhibit*, Reno, NV, Jan. 2003, AIAA 2003-421.
[18] K. A. Harper, M. D. Berkemeier, and S. Grace, "Modeling the dynamics of spring-driven oscillating-foil propulsion," *IEEE J. Oceanic Eng.*, vol. 23, pp. 285–296, July 1998.
[19] S. N. Singh and A. Simha, "Open-loop and feedback pectoral fin control of biorobotic AUV," presented at the Int. Symp. Untethered Submersible Technology (UUST03), Durham, NH, 2003.
[20] S. N. Singh and W. J. Rugh, "Decoupling in a class of nonlinear systems by state variable feedback," *Trans. ASME J. Dynam. Syst., Measurem., Control*, vol. 94, pp. 323–329, 1972.
[21] A. Isidori, *Nonlinear Control Systems*. New York: Springer-Verlag, 1989.
[22] J.-J. E. Slotine and W. Li, *Applied Nonlinear Control*. Englewood Cliffs, NJ: Prentice-Hall, 1991.
[23] L. Benvenut, M. D. DI. Bendetto, and J. W. Grizzle, "Approximate output tracking for nonlinear nonminimum phase system with an application to flight control," *Int. J. Robust Nonlinear Control*, vol. 4, pp. 397–414, 1994.
[24] R. Cristi, F. A. Papoulias, and A. J. Healy, "Adaptive sliding mode control of autonomous underwater vehicles in the dive plane," *IEEE J. Oceanic Eng.*, vol. 15, pp. 152–160, July 1990.
[25] S. N. Singh and L. Wang, "Output feedback form and adaptive stabilization of a nonlinear aeroelastic system," *J. Guidance, Control, Dynam.*, vol. 25, no. 4, pp. 725–733, 2002.
[26] C. P. Ellington, "The aerodynamics of hovering insect flight," *Philos. Trans. R. Soc. Lond., B*, vol. 305, pp. 79–113, 1984.
[27] M. H. Dickinson, F. O. Lehmann, and S. P. Sane, "Wing rotation and the aerodynamic basics of insect flight," *Sci.*, vol. 284, pp. 1954–1960, 1999.
[28] M. Triantafyllou, A. Techet, and F. Hover, "Review of experimental work in biomimetic foils," presented at the 13th Int. Symp. Unmanned Untethered Submersible Technology (UUST), Durham, NH, Aug. 2003.
[29] R. Mittal, "Computational modeling in bio-hydrodynamics: Trends, challenges and recent advances," presented at the 13th Int. Symp. Unmanned Untethered Submersible Technology (UUST), Durham, NH, Aug. 2003.
[30] H. H. Rosenbrock, *State-Space and Multivariable Theory*. New York: Wiley, 1970.
[31] T. Kailath, *Linear Systems*. Englewood Cliffs, NJ: Prentice-Hall, 1980.
[32] M. M. Koochesfahani, "Vertical patterns in the wake of an oscillating airfoil," presented at the AIAA 25th Aerospace Sciences Meeting and Exhibit, Reno, NV, Jan. 1987, AIAA 87-0111.

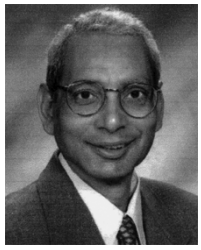

Sahjendra N. Singh (M'78–SM'86) received the M.E. degree (with distinction) in applied electronics and servomechanism from the Indian Institute of Science, Bangalore, India, in 1968 and the Ph.D. degree in electrical engineering from The Johns Hopkins University, Baltimore, MD, in 1972.

He currently is a Professor in the Department of Electrical and Computer Engineering, University of Nevada, Las Vegas (UNLV). Prior to coming to UNLV in 1986, he did research at the Indian Space Research Organization and the National Aeronautics and Space Administration (NASA) Langley Research Center in the areas of space vehicle stability and control, space robotics, flight control systems, and control of large space structures. He has done research at the Air Force Research Laboratory, Edwards Air Force Base, CA; the Naval Air Warfare Center, Warminster, PA; the Naval Undersea Warfare Center, Newport, RI; the Naval Air Warfare Center, Patuxent, MD; the Air Force Research Laboratory, Wright-Patterson Air Force Base; and the NASA Dryden Flight Research Center, Edwards, as a NASA and Office of Naval Research Summer Faculty Fellow in the areas of flight control of advanced fighter aircraft, nonlinear systems, adaptive and neural control, turbulence control, and biologically inspired maneuvering of agile undersea vehicles, formation flying of UAVs, and aeroelasticity and control. He has published over 250 journal and conference papers in these areas. He has served as an Associate Editor for the *Journal of Guidance, Control, and Dynamics*.

Dr. Singh is an Associate Fellow of the American Institute of Aeronautics and Astronautics (AIAA).

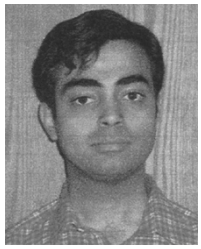

Aditya Simha (S'02) received the B.S. degree in electrical and electronics engineering from Visveswaraiah Technological University, India, in 2002 and is currently working toward the M.S. degree in electrical engineering at the University of Nevada, Las Vegas.

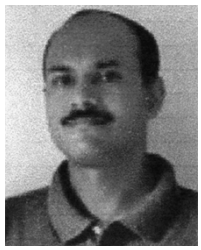

Rajat Mittal was born in New Delhi, India, on April 6, 1967. He received the B.Tech. degree in aeronautical engineering from the Indian Institute of Technology, Kanpur, in 1989, the M.S. degree in aerospace engineering from the University of Florida, Gainesville, in 1991, and the Ph.D. degree in applied mechanics from The University of Illinois, Urbana-Champaign, in 1995.

He joined the Center for Turbulence Research, Stanford University, Stanford, CA, as a Postdoctoral Fellow, where he conducted research in the area of turbulent flows. Subsequently, he joined the Department of Mechanical Engineering, University of Florida, as an Assistant Professor, where he taught from 1996 to 2001. He currently is an Associate Professor in the Department of Mechanical and Aerospace Engineering, The George Washington University, Washington, DC. His research interests include computational fluid dynamics, vortex dominated flows, fluid-structure interaction, flow control, and biofluid dynamics.

Dr. Mittal is a Member of the American Institute of Aeronautics and Astronautics, the American Society of Mechanical Engineers, and the American Physical Society.